NANO LETTERS
2007
Vol. 7, No. 10
3051−3055

Three-Dimensional Morphology of GaP–GaAs Nanowires Revealed by Transmission Electron Microscopy Tomography

Marcel A. Verheijen,[*,†] Rienk E. Algra,[†,‡,§] Magnus T. Borgström,[†] George Immink,[†] Erwan Sourty,[||] Willem J. P. van Enckevort,[§] Elias Vlieg,[§] and Erik P. A. M. Bakkers[†]

Philips Research Laboratories Eindhoven, High Tech Campus 11, 5656AE Eindhoven, The Netherlands, Nederlands Institute for Material Research (NIMR), 2628CD Delft, The Netherlands, IMM, Solid State Chemistry, Radboud University Nijmegen, Toernooiveld 1, 6525ED Nijmegen, The Netherlands, and FEI Company, Achtseweg Noord 5, Building AAE, 5600 KA Eindhoven/Acht, The Netherlands

Received June 28, 2007; Revised Manuscript Received August 28, 2007

ABSTRACT

We have investigated the morphology of heterostructured GaP–GaAs nanowires grown by metal–organic vapor-phase epitaxy as a function of growth temperature and V/III precursor ratio. The study of heterostructured nanowires with transmission electron microscopy tomography allowed the three-dimensional morphology to be resolved, and discrimination between the effect of axial (core) and radial (shell) growth on the morphology. A temperature- and precursor-dependent structure diagram for the GaP nanowire core morphology and the evolution of the different types of side facets during GaAs and GaP shell growth were constituted.

Semiconductor nanowires are promising candidates for enabling integration of new functionalities[1−4] based on the advantageous properties of III−V semiconductors, such as high carrier mobility and optical activity into existing silicon technology.[5−8] Because of the small dimensions and the consequently large ratio of surface to bulk atoms, the nanowire surface morphology and resulting chemistry can considerably affect the nanowire (opto-) electronic properties, such as carrier mobility[9] and luminescence quantum yield.[10,11] An elegant way to suppress such surface related effects is to cap the wires with a wide band gap material to form core/shell[12−15] nanowire structures. So far, only the vapor−liquid−solid (VLS), i.e., the axial growth mechanism and the zinc blende crystal structure, has been considered in relation to the III−V nanowire side faceting.[16−19] In order to design and optimize nanowire properties for optical, electrical, or mechanical performance, it is essential to take control over the nanowire surface morphology by fully understanding the parameters affecting radial growth.

* Corresponding author. E-mail: m.a.verheijen@philips.com.
† Philips Research Laboratories Eindhoven.
‡ Nederlands Institute for Material Research (NIMR).
§ IMM, Solid State Chemistry, Radboud University Nijmegen.
|| FEI Company.

In this paper we demonstrate the versatility of three-dimensional (3D) transmission electron microscopy (TEM) tomography, allowing the study of facet formation during radial overgrowth and the complex behavior of nanowire morphology as a function of precursor molar fractions and growth temperature. Furthermore, we make a distinction between the morphology determined by the axial VLS growth and the morphology introduced by additional radial (non-VLS) "side-wall" growth.

Axial multisegment GaP−GaAs heterostructure nanowires were synthesized on oxidized Si substrates in an Aixtron 200 MOVPE reactor, as previously described in reports on growth kinetics[15] and heterostructure interfaces[20] of these nanowires. By means of switching of the precursor gases, alternating segments of GaP and GaAs were grown as a single-crystalline structure (see Figure S1). It is essential to realize that during vertical (VLS) growth of the nanowire, radial epitaxial sidewall growth also occurs (see Figure S2). Therefore, the alteration of precursor gases introduces a series of shells of alternating composition. All samples were studied with a FEI Tecnai 300 kV TEM in bright field, high-resolution TEM (HRTEM) as well as in high-angle annular dark field (HAADF) mode. Scanning TEM (STEM) tomography was performed using the automated tilt-series acquisi-

10.1021/nl071541q CCC: $37.00 © 2007 American Chemical Society
Published on Web 09/21/2007

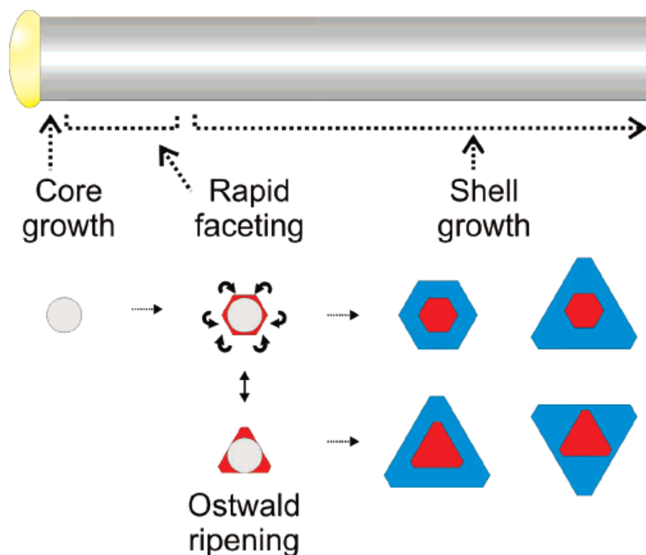

Figure 1. Schematic model for facet development on nanowires. A core with a spherical cross section is precipitated directly from the catalyst particle. Within a few seconds after the formation of the core, facets develop by fast lateral growth of the kinked surface. Subsequent shell growth will determine the resulting overall morphology. Alternatively, Ostwald ripening (due to fast surface diffusion) may alter the surface areas of the facets before shell growth initiates.

tion software Xplore3D on a FEI Tecnai F20 X-Twin operated at 200 kV. HAADF images were acquired at 2° tilt intervals in a tilt range of −68° to +68° using a Fischione single tilt tomography holder. Data processing and visualization were performed using Inspect3D and Amira, respectively (Xplore3D software suite). We address the morphology of ⟨111⟩ grown wires with twin boundaries oriented perpendicular to the VLS growth direction only but note that about 5% of the characterized wires exhibited a ⟨112⟩ growth direction. The latter growth direction only appeared in restricted sections of the wires bounded by kinked transitions to ⟨111⟩ grown sections.

Nanowire core morphologies were determined from the orientation of the side facets just below (<100 nm) the gold particle and precisely at a GaP/GaAs heterojunction in tomography studies. Here, the effects of sidewall growth are minor because of the short exposure time of the facets to the supply of growth units and the low radial growth rates in the temperature range 460 °C < T < 530 °C.[15] Assuming a semidome shape of the liquid gold droplet (due to the surface tension), one would expect a circular cross section of the wire close to the interface with the gold droplet, as depicted at the left portion of Figure 1. However, side view HAADF and tomography studies revealed symmetrically nonequivalent facets at the heterojunction interfaces and at the first 10 nm below the top of the wire, respectively. We explain the formation of a noncircular cross section by rapid faceting of high index sidewall orientations. This faceting occurs within a few seconds after nanowire precipitation from the catalyst particle (see Figure 1). After the facet formation, shell growth will determine the overall morphology. Alternatively, Ostwald ripening (specifically observed when using high or low V/III ratios) may alter the surface areas of the facets close to the top of the nanowire before shell growth has initiated. Less stable facets disappear in favor of the more stable facets, since surface diffusion is fast at these length scales and at these temperatures (Figure 1). In the rest of this paper we refer to the morphology obtained after rapid faceting and possible Ostwald ripening as the "core morphology". In the following we discuss the GaP core morphology. GaAs core morphology results are found in the Supporting Information. In the last section shell growth on the different core morphologies will be investigated.

In order to understand the mechanism behind the different nanowire core morphologies, wires grown at different temperatures and precursor flows were characterized. All wires were studied in TEM by tilting it around its long axis. When the wire was viewed along the $\langle 11\bar{2}\rangle$ direction, straight sidewalls running parallel to the long axis of the wire were observed for all growth conditions, in agreement with previous studies.[16] However, when the wire was viewed along the $\langle \bar{1}10\rangle$ direction, a growth parameter dependent morphology was observed. The obtained morphologies are summarized in the *structure diagram* in Figure 2. At temperatures below 500 °C, the GaP segments show the zinc blende crystal structure, whereas at higher temperatures a mixture of domains with zinc blende and wurtzite are observed. In total, five different types of nanowire morphologies could be discriminated, which are all represented in Figure 3 and will be discussed separately below:

(Type 1). For wires grown at low growth temperatures (400 °C < T ≤ 460 °C) and low V/III precursor flow ratios (≤9), a zigzag pattern of nonparallel facets bounded at the twin boundaries is visible upon viewing along the $\langle \bar{1}10\rangle$ direction (see Figure S3a in Supporting Information). The wire is terminated by {111} facets, in accordance with literature.[16]

(Type 2). At higher growth temperatures (460 °C < T < 530 °C) wires with straight edges were observed for both the $\langle \bar{1}10\rangle$ and $\langle 11\bar{2}\rangle$ viewing directions (as represented by the high-resolution TEM image in Figure S3b in Supporting Information). In this case, additional HRTEM imaging of cross-sectional samples showed that the GaP nanowire core has six {112} side facets.[15] This 6-fold symmetry cross section is predominant (see Figures 2 and 3) only at 460 and 480 °C, and intermediate V/III ratios.

(Types 2′ and 2″). Interestingly, for higher V/III ratios at 460 °C and at higher growth temperatures (460 °C < T < 530 °C) one of the two types of {112} facets becomes more stable, leading to a 3-fold symmetry with three larger and three smaller {112} facets. This morphology was confirmed by HAADF imaging upon viewing along the $\langle \bar{1}10\rangle$ direction close to the top. The intensity profiles across the wire were consistent with a 3-fold symmetry shape (see Figure S4).

The variation in stability of the two types of {112} side facets as a function of group V overpressure can be explained by the polar nature of these facets. An increased concentration of active P, induced by the temperature and/or PH_3 flow, will stabilize the P-terminated $\{112\}_B$ facets, resulting in a cross-sectional shape with larger $\{112\}_B$ than $\{112\}_A$ planes. This is consistent with the 6-fold to 3-fold morphology

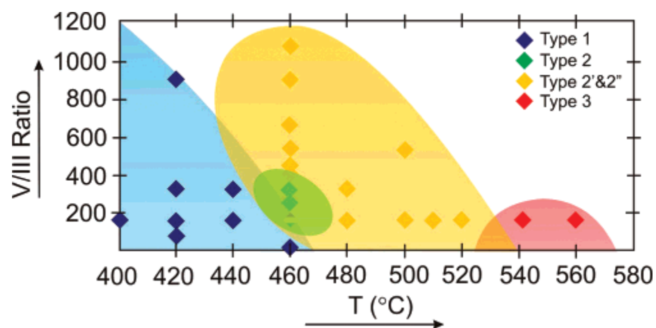

Figure 2. GaP core morphologies as a function of temperature and V/III precursor flow ratio. For each data point 3−12 wires have been investigated using side view bright field TEM and HAADF imaging along the ⟨$\bar{1}$10⟩ zone axis. The colored areas suggest parameter spaces of the various morphologies. Type 1 represents wires with $\{111\}_A$ and $\{111\}_B$ facets yielding a 3-fold symmetry cross section. Type 2 wires have $\{112\}_A$ and $\{112\}_B$ facets of roughly equal size providing a hexagonal cross section. Type 2′ and 2″ wires have $\{112\}_A$ and $\{112\}_B$ facets with unequal surface area yielding a 3-fold symmetry cross section. Note that at 460 °C and V/III ratio = 163, three different morphologies were observed. Here {111} and {112} side faceting was observed for low and high PH_3 flows, respectively, indicating that the absolute gas flows determined the morphology.

change as a function of temperature. In the temperature regime used for our experiments, the PH_3 pyrolysis in presence of III−V material (in this case the nanowire) increases superlinearly with temperature,[21] which indicates that the V/III ratio is the only parameter that shows a systematic correlation to the morphology changes. This is indicated in Figure 3 by the two alternatives 2′ and 2″.

(Type 3) In the temperatures range 530 °C $< T <$ 560 °C, the GaP segments contain a mixture of zinc blende and wurtzite domains. Both have 6-fold symmetry and they are bounded by six {112} facets (Figure 3) and six {100} facets, respectively. The facet orientation of the wurtzite segments was deduced from the equivalent orientation in the zinc blende domains.

The morphology determining parameter for the formation of type 1, 2, or 3 is temperature. This can be understood from the temperature dependence of the dominant mechanism for thin film growth: In the temperature range 400−460 °C, sidewall growth is limited by a thermally activated process,[15] most likely being the incorporation of growth units at step edges, leading to the formation of flat facets. In this case the most stable facets, being the {111} facets, will dominate the growth form. In the temperature range 460−520 °C sidewall growth becomes a diffusion-limited process.[15] Facets parallel to the growth direction are now more likely to develop.

3D TEM tomography images of the bottom part of a nanowire are shown in Figure 4. The complete dataset of images is available as a movie as Supporting Information. The structure encloses a GaP core (first segment grown on the substrate) and a GaAs core (second segment). Two nanometer thick slices through the 3D data set from the GaP core segment are shown in parts c and d of Figure 4 and from the GaAs core segment in parts e and f of Figure 4. Examination of successive slices showed that the GaP core is defined by two sets of symmetrically nonequivalent facets differing slightly in surface area, which was confirmed by additional cross-sectional studies on other wires from the same sample. The contrast change as a function of wire diameter shows the presence of a sequence of GaAs and GaP shells, similar to previously observed nanowire cross sections (see Figure S2).[15] Thus, the heterostructured nature of the wires enables us to discriminate between morphology induced by axial (core) and radial (shell) growth. While the overall morphology could be obtained from high-resolution scanning electron microscopy (SEM) images (see Figure S6), this technique does not reveal the "inside" of the wires as powerfully demonstrated with TEM tomography.

Although the radial growth rate is typically 2 orders of magnitude lower than the axial growth rate, sidewall growth can substantially affect the nanowire outer morphology. Therefore, in addition to tomography characterization both side view and cross-sectional studies were performed for the two most important regimes (types 1 and 2). In side view TEM studies of the wires, the nanowire faceting was studied at different positions along the wire. For the type 1 GaP segments, grown in the kinetically limited regime, no change in morphology as a function of radial overgrowth was observed. Radial growth is continued on the {111} facets formed during axial growth, which is in line with kinetically controlled growth in this temperature regime.

The GaP type 2 core segments terminated by {112} facets, grown in the diffusion-limited regime, showed a more complex behavior and developed nonparallel side facets upon additional sidewall growth. This is illustrated by the tomography image in Figure 4g showing the evolution from a straight GaP core with {112} facets to a shell with many nanofacets. The axial outer morphology, as defined by newly emerging facets resulting from mainly GaAs radial overgrowth is strongly dependent on the density of twin boundaries in the wires. For low twin densities and large twin domains, the evolution of parallel {112} facets into nonparallel facets implies the appearance of at least two types of subfacets with opposing tilts with respect to the parallel orientation. One of the two sets of {112} facets breaks up into {111} and {200} facets, whereas the {112} facets of opposite polarity remain flat, introducing the asymmetry in the morphology, (see Figure S5 in Supporting Information), and previously observed for Si[22] and GaAs.[23] For high twin densities and small twin domains, in the order of a few nanometers in length, {200} facets do not form, and {111} nanofacets bound by twin planes determine the morphology of the former {112} facets. The ability to create thin slices from the tomography data (parts c−f of Figure 4) allows the visualization of the morphology of individual twin domains, which reveals further complexity in the detailed radial growth behavior. The symmetry of the ⟨111⟩ long axis of the wire and its outer morphology is 3-fold rather than 6-fold, in accordance with the polarity-dependent facet evolution of the polar {112} facets. Strikingly, close inspection of parts c and d of Figure 4 shows that the nanowire morphology is inversed by radial overgrowth, i.e., the less

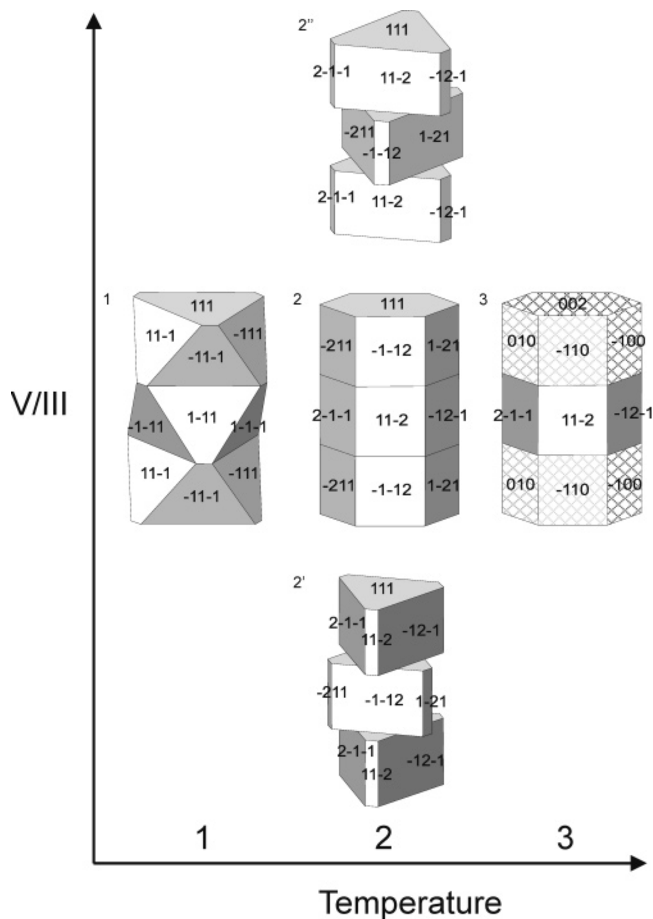

Figure 3. Schematic 3D representation of the various VLS GaP core morphologies. Morphology types 1, 2″, 2, and 2′ represent zinc blende crystal structures, while type 3 shows the morphology of alternating zinc blende and wurtzite segments in high-temperature grown wires (the shaded parts represent the Wurtzite structure). Note that for type 2 and 3 rotational stacking faults do not affect the outer morphology.

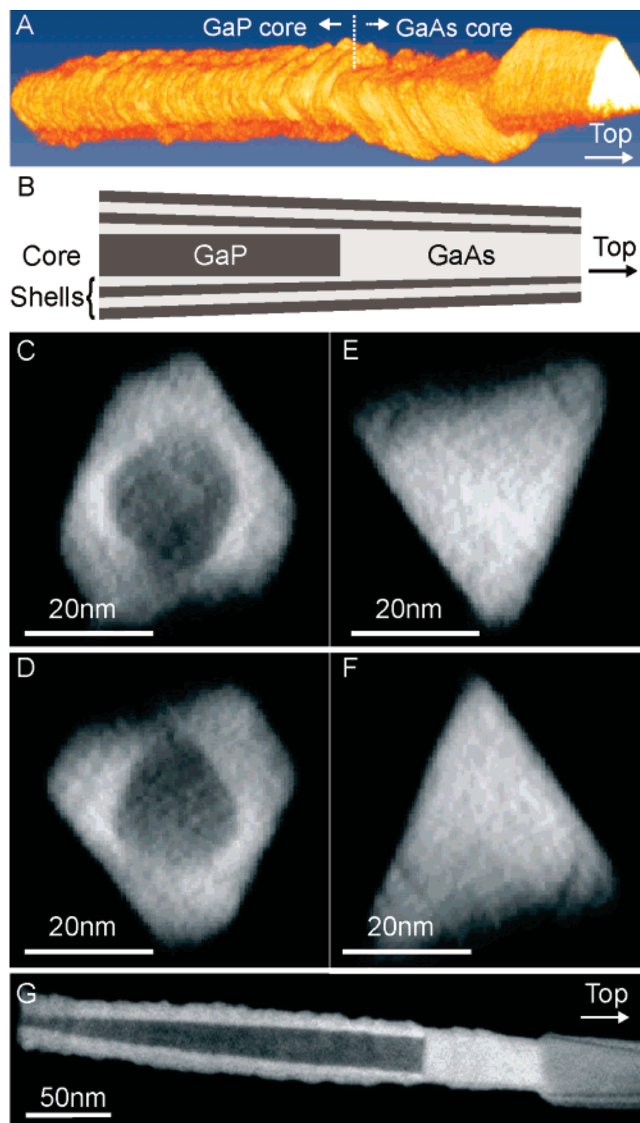

Figure 4. (A) 3D reconstruction of the morphology of the bottom part of a GaP−GaAs heterostuctured nanowire (grown at 480 °C, molar fractions of TMG, PH_3, and AsH_3: 7.3×10^{-5}, 1.5×10^{-2}, and 1.5×10^{-2}, respectively). (B) Schematic drawing of the part of the heterostructured nanowire shown in A. Arrows indicate the growth direction. Figures C/D and E/F show cross-sectional slices of the two differently oriented twin domains in the GaP-core segment and GaAs segment, respectively. (G) Cross-sectional view sliced along the length direction of the wire, displaying the sharp interface between the GaP (dark) and GaAs (light) core segments and the core/shell structure. The GaP core has facets parallel to the long axis while the outer surface of the shell has nonparallel facets. (This sliced view was made with a small inclination with respect to the length direction, yielding the nonrectangular shape of the GaP core on the left.)

stable set of {112} facets of the GaP core (the facets with smallest surface area) are the more stable ones on the GaAs shell, and vice versa. The observation of growth parameter dependent stability reversal of the two polar {112} facets prior to thickening of the nanowires implies an originally cylindrical core shape, since only then both polarities can be formed. On the other hand, for the segment with a GaAs core, no reversal in polarity stability is observed. The explanation can be found in the more efficient pyrolysis of AsH_3[24] than that of PH_3[21] at the growth temperatures used. The effectively higher As pressures enable faster incorporation of As growth units on the (Ga-terminated) $\{112\}_A$ facets which decrease in size in favor of the (As-terminated) $\{112\}_B$ facets for core as well as shell growth, similar to reports on mesa growth.[25] For thick enough shells, consisting of mainly GaAs, the $\{112\}_A$ facets grow out completely. Finally, regarding the morphology reversal between GaP core and (mainly GaAs) shell, we have shown that a $\{112\}_A$ faceted GaP core can be obtained using low active P pressures leading to less stable $\{112\}_B$ facets. In contrast, we anticipate that the $\{112\}_B$ facets will become dominant on the GaP core at higher temperatures and high PH_3 overpressures.

In summary, we have used a powerful TEM tomography technique to reveal the three-dimensional morphology of heterostructured GaP−GaAs nanowires. Importantly, we showed that the faceting of the GaAs and GaP segments is determined by differences in growth kinetics of different crystallographic faces and can be tuned by the temperature and precursor V/III ratio. We demonstrated that low growth temperatures yield nonparallel {111} side facets and high growth temperatures create parallel {112} facets. The precur-

sor ratio determines the cross sectional shape of these wires to have either pseudohexagonal or 3-fold symmetry. For GaP nanowires, the relative size of $\{112\}_A$ and $\{112\}_B$ facets appears to be temperature dependent. These results present a fundamental advance in the general understanding of nanowire facet formation and will allow optimizing fabrication conditions for nanowires with smooth surfaces.

Acknowledgment. This research was carried out under project number MC3.05243 in the framework of the Strategic Research programme of The Netherlands Institute for Metals Research in The Netherlands (www.nimr.nl), the European Marie Curie program, the European FP6 NODE (015783) project, and the ministry of economic affairs of The Netherlands (NanoNed).

Supporting Information Available: Images of a GaP-GaAs-GaP heterointerface, heterostructured GaP-GaAs nanowire, upper GaP segments of GaP/GaAs wires, and a wire grown at 520 °C and video of GaAs core morphology. This material is available free of charge via the Internet at http://pubs.acs.org.

References

(1) Huang, M. H.; et al. Room-temperature ultraviolet nanowire nanolasers. *Science* **2001**, *292*, 1897−1899.
(2) Zheng, G. F.; Patolsky, F.; Cui, Y.; Wang, W. U.; Lieber, C. M. Multiplexed electrical detection of cancer markers with nanowire sensor arrays. *Nat. Biotechnol.* **2005**, *23*, 1294−1301.
(3) Borgstrom, M. T.; Zwiller, V.; Muller, E.; Imamoglu, A. Optically bright quantum dots in single nanowires. *Nano Lett.* **2005**, *5*, 1439−1443.
(4) van Dam, J. A.; Nazarov, Y. V.; Bakkers, E. P. A. M.; De Franceschi, S.;Kouwenhoven, L. P. Supercurrent reversal in quantum dots. *Nature* **2006**, *442*, 667−670.
(5) Bakkers, E. P. *et al.* Epitaxial growth of InP nanowires on germanium. *Nat. Mater.* **2004**, *3*, 769−773.
(6) Martensson, T. *et al.* Epitaxial III-V nanowires on silicon. *Nano Lett.* **2004**, *4*, 1987−1990.
(7) Kamins, T. I.; Li, X.; Williams, R. S. Growth and structure of chemically vapor deposited Ge nanowires on Si substrates. *Nano Lett.* **2004**, *4*, 503−506.
(8) Bakkers, E. P. A. M.; Borgstrom, M. T.; Verheijen, M. A. Epitaxial growth of III-V nanowires on group IV substrates. *MRS Bull.* **2007**, *32*, 117−122.
(9) Li, Y.; et al. Dopant-free GaN/AlN/AlGaN radial nanowire heterostructures as high electron mobility transistors. *Nano Lett.* **2006**, *6*, 1468−1473.
(10) van Weert, M. H. M.; et al. Large redshift in photoluminescence of p-doped InP nanowires induced by Fermi-level pinning. *Appl. Phys. Lett.* **2006**, *88*.
(11) van Vugt, L. K.; Veen, S. J.; Bakkers, E. P. A. M.; Roest, A. L.; Vanmaekelbergh, D. Increase of the photoluminescence intensity of InP nanowires by photoassisted surface passivation. *J. Am. Chem. Soc.* **2005**, *127*, 12357−12362.
(12) Lauhon, L. J.; Gudiksen, M. S.; Wang, C. L.; Lieber, C. M. Epitaxial core-shell and core-multishell nanowire heterostructures. *Nature* **2002**, *420*, 57−61.
(13) Skold, N.; et al. Growth and optical properties of strained GaAs-GaxIn1-xP core-shell nanowires. *Nano Lett.* **2005**, *5*, 1943−1947.
(14) Li, H. Y.; et al. Remote p-Doping of InAs Nanowires. *Nano Lett.* **2007**, *7*, 1144−1148.
(15) Verheijen, M. A.; Immink, G.; deSmet, T.; Borgstrom, M. T.; Bakkers, E. P. A. M. Growth Kinetics of Heterostructured GaP-GaAs Nanowires. *J. Am. Chem. Soc.* **2006**, *128*, 1353−1359.
(16) Johansson, J.; et al. Structural properties of (111)B-oriented III-V nanowires. *Nat. Mater.* **2006**, *5*, 574−580.
(17) Wacaser, B. A.; Deppert, K.; Karlsson, L. S.; Samuelson, L.; Seifert, W. Growth and characterization of defect free GaAs nanowires. *J. Cryst. Growth* **2006**, *287*, 504−508.
(18) Plante, M. C.; LaPierre, R. R. Growth mechanisms of GaAs nanowires by gas source molecular beam epitaxy. *J. Cryst. Growth* **2006**, *286*, 394−399.
(19) Persson, A. I.; Ohlsson, B. J.; Jeppesen, S.; Samuelson, L. Growth mechanisms for GaAs nanowires grown in CBE. *J. Cryst. Growth* **2004**, *272*, 167−174.
(20) Borgstrom, M. T.; Verheijen, M. A.; Immink, G.; de Smet, T.; Bakkers, E. P. A. M. Interface study on heterostructured GaP-GaAs nanowires. *Nanotechnology* **2006**, *17*, 4010−4013.
(21) Larsen, C. A.; Buchan, N. I.; Stringfellow, G. B. Mass-Spectrometric Studies of Phosphine Pyrolysis and Omvpe Growth of InP. *J. Cryst. Growth* **1987**, *85*, 148−153.
(22) Ross, F. M.; Tersoff, J.; Reuter, M. C. Sawtooth faceting in silicon nanowires. *Phys. Rev. Lett.* **2005**, *95*,.
(23) Zou, J. *et al.* Growth mechanism of truncated triangular III-V nanowires. *Small* **2007**, *3*, 389−393.
(24) Li, S. H.; Larsen, C. A.; Stringfellow, G. B. Decomposition Mechanisms of Trimethylarsine. *J. Cryst. Growth* **1990**, *102*, 117−125.
(25) Asai, H. Anisotropic Lateral Growth in GaAs MOCVD Layers on (001) Substrates. *J. Cryst. Growth* **1987**, *80*, 425−433.

NL071541Q